JACS
JOURNAL OF THE AMERICAN CHEMICAL SOCIETY

ARTICLE

pubs.acs.org/JACS

Measurements and Modeling of Recombination from Nanoparticle TiO_2 Electrodes

Jesse W. Ondersma and Thomas W. Hamann*

Department of Chemistry, Michigan State University, East Lansing, Michigan 48824-1322, United States

Supporting Information

ABSTRACT: Electron-transfer reactions from nanoparticle TiO_2 films to outer-sphere redox shuttles were investigated. Steady-state dark current density versus applied potential and open circuit voltage decay measurements were employed to determine the rates of recombination to cobalt(III) tris(4,4′-dimethyl-2,2′-bipyridyl), $[Co(Me_2bpy)_3]^{3+}$, and ruthenium(III) bis(2,2′-bipyridyl)-bis(*N*-methylimidozole), $[Ru(bpy)_2(MeIm)_2]^{3+}$. A striking difference in the magnitude as well as the shape of the electron lifetimes for TiO_2 electrodes in contact with these two redox shuttles is observed. A model based on Marcus theory is developed to describe recombination, including contributions from conduction band electrons and surface states. Excellent agreement was found between the modeled and measured lifetimes. The model allows for identification of each contributing component of electron transfer to the measured lifetimes. Comparison of the different components of the modeled lifetimes to the measured lifetimes provides clear evidence for recombination mediated through surface states.

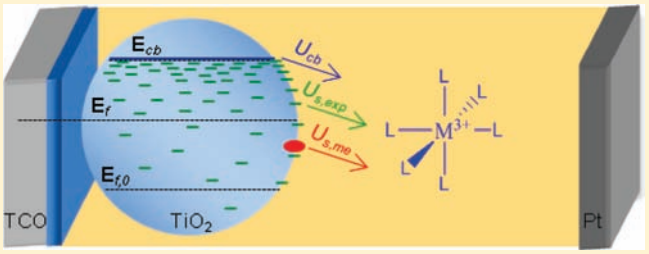

INTRODUCTION

In 1991, O'Regan and Grätzel published a breakthrough report on using high surface area nanoparticle TiO_2 electrodes in dye-sensitized solar cells, DSSCs, to increase the light harvesting of a ruthenium-based molecular dye in contact with an I_3^-/I^- redox shuttle.[1] The energy conversion efficiency of DSSCs was rapidly improved over the next 2 years to 10%, primarily due to the development of the N3 dye, $[Ru(4,4'\text{-dicarboxy-}2,2'\text{-bipyridine})_2(NCS)_2]$.[2] Despite intensifying research efforts over the following 18 years, the maximum efficiency essentially plateaued at 11%.[3,4] Despite the lack of improved efficiency over this period, intense study by research groups around the world has led to greatly improved understanding of the operational principles of DSSCs.[5−11]

The largest loss mechanism in state-of-the-art DSSCs is the overpotential required for efficient dye regeneration by iodide.[12] One strategy to significantly improve the efficiency is therefore replacing I_3^-/I^- with a redox shuttle with a more positive potential. To date, however, this strategy has not led to improved performance due to the concomitant increasing rate of recombination of photoinjected electrons from TiO_2 to the oxidized form of the redox shuttle.[12−15] Development of alternative redox shuttles, which are not hampered by fast recombination, should be facilitated by a detailed understanding of this reaction. Several important details of the recombination mechanism are still not established, however, which is largely due to continued reliance on I_3^-/I^- as the redox shuttle.[11] For example, the acceptor species involved in recombination, either I_2 or I_3^-, is not definitively established.[16] We note that an analysis of several proposed recombination mechanisms to I_3^-/I^- has recently been presented elsewhere.[6] Another interesting ongoing discussion involving recombination is the extent to which surface states participate. Because the environment of surface atoms of the TiO_2 film is inherently unique from that in the bulk, there will be localized electronic states on the surface. If these states are energetically located between the redox level of the redox shuttle in the electrolyte and the conduction band energy, it is possible that they participate in recombination. Therefore, to fully understand recombination, the role of surface states must be understood.

Recombination is most often discussed in terms of electron lifetimes: the average time an electron "lives" in the TiO_2 electrode before being captured by an acceptor in the electrolyte. Lifetimes have been measured by a variety of methods including intensity modulated photovoltage spectroscopy, open-circuit voltage decay, and impedance spectroscopy.[9,17,18] It has been well-established that the electron lifetime has an exponential dependence on potential.[19,20] This dependence has been explained on the basis of electronic processes happening prior to electron transfer to the redox shuttle. The model, the multiple-trapping model, considers that TiO_2 contains a large number of electron traps and a low number of free electrons. Thus, before a recombination event may occur, an electron must become excited from a trap state into the conduction band before traveling to the surface of the nanoparticle. So the lifetime increases as the ratio of trapped to free electrons increases, which changes exponentially as the Fermi level moves through the band gap.[18,19] This exponential dependence holds true only when recombination is occurring primarily from the conduction band. Recent reports, however, have provided indirect evidence of surface state-mediated recom-

Received: February 11, 2011
Published: May 11, 2011

dx.doi.org/10.1021/ja201333u | J. Am. Chem. Soc. 2011, 133, 8264–8271

bination.[15,21] The signature of surface state-mediated recombination is a parabolic component in the electron lifetime, a deviation of log−linear behavior observed for conduction band recombination.[9,22] For example, when an aqueous polysulfide electrolyte was used in a quantum dot-sensitized solar cell, a deviation of the exponential dependence of the lifetime indicated surface state-mediated recombination.[9,23] However, interpretation of the recombination mechanism with this electrolyte is complicated by use of the inner-sphere, multielectron acceptor, and the uncertain effect of the quantum dot and solvent on the measured lifetime.

A better picture of recombination kinetics from TiO_2 can be established by eliminating the complicated electrochemistry of the I_3^-/I^- redox shuttle. For example, using a simple outer-sphere redox shuttle ensures that a single one-electron acceptor species is in solution.[11] Further, use of such redox shuttles offers the ability to tune the physical parameters, such as redox potential and reorganization energy, allowing systematic studies that are not possible with I_3^-/I^-. In addition to being excellent model systems, recent reports have indicated that outersphere redox shuttles may be used to produce high-efficiency DSSCs.[24,25] Recently, we utilized a series of cobalt bipyridyl redox shuttles to investigate the bottlenecks, which can limit the efficiency of outersphere redox shuttles in DSSCs.[26,27] On the basis of these results, we concluded that surface states do not appear to play a role in recombination.[26] We reasoned that, to definitively observe whether recombination occurs via surface states, it would have to be faster than recombination from the conduction band. In this work, therefore, we set out to achieve this by comparing recombination to redox shuttles with vastly different redox potentials and reorganization energies. We then develop a model based on Marcus theory to describe recombination, considering contributions from both conduction band and surface states. The combined experimental and modeling results allow us to clearly identify each separate element of recombination.

EXPERIMENTAL SECTION

All working electrodes utilized either a TiO_2 or a poly phenyl oxide, PPO, blocking layer to prevent complications associated with electron transfer from the substrate (i.e., shunting) and ensure the measured recombination was strictly from the nanoparticle film.[13,27,28] A detailed comparison of the different blocking layers is forthcoming; however, the blocking layers used in this study do not affect the analysis presented herein.[13,15,29] Nanoparticle TiO_2 electrodes utilizing a dense blocking layers of TiO_2 were prepared as described previously, with the exception of using Ti-nanoxide T20 paste (Solaronix).[26] The TiO_2 film thickness, d, was measured using a Dektak3 Surface Profiler to be 8 μm. For electrodes utilizing a poly phenol oxide (PPO) blocking layer, the PPO was selectively polymerized onto the bare FTO after the nanoparticle TiO_2 film was deposited onto FTO and annealed as described above. Electropolymerization was carried out following the reported procedure of Gregg et al.[13] Briefly, the electrodes were submerged in a solution of 60 mM phenol, 90 mM 2-allylphenol, 100 mM $LiClO_4$ in a 10/10/1 water/ethanol/2-butoxyethanol solvent mixture adjusted to pH 9 by addition of 10 mM tetrabutylammonium hydroxide in methanol. The potential of the electrodes was then scanned from 0 to 1.5 V vs SCE at a rate of 100 mV/s for 60−80 cycles. The electrodes where then soaked in 10 mM tetrabutylammonium hydroxide in methanol to remove unreacted monomers and oligomers, rinsed with ethanol, and cured in air at 150 °C for 30 min. The electropolymerization process is self-limiting and deposits only on the conductive FTO substrate because the TiO_2 is insulating at the potentials used. Sandwich DSSCs were fabricated according to a previously described procedure.[26] Three-electrode measurements were made in a custom electrochemical cell.[26] The photoanode was clamped over an opening in the cell and sealed with a Viton O-ring. A commercial AgCl/Ag reference electrode (ESA 66-EE009 "No Leak") was used for all three-electrode measurements. The counter electrode consisted of a high surface area platinum mesh.

Ruthenium(II) bis(2,2′-bipyridyl)-bis(*N*-methylimidozole) hexafluorophosphate, $[Ru(bpy)_2(MeIm)_2](PF_6)_2$, was prepared following a literature procedure.[30] The resulting product was purified on an activated neutral alumina column using acetonitrile as the eluent. The cobalt outer-sphere redox couple employed in this study, cobalt(II) tris(4,4′-dimethyl-2,2′-bipyridyl) hexafluorophosphate, $[Co(Me_2bpy)_3](PF_6)_2$, was prepared as described previously.[27] All electrolytes contained 0.1 M $LiClO_4$ and 40 M of either $[Co(Me_2bpy)_3](PF_6)_2$ or $[Ru(bpy)_2(MeIm)_2](PF_6)_2$ in acetonitrile. Sufficient $NOBF_4$ was added from a stock solution to each electrolyte to oxidize 20 mM of the redox shuttle unless otherwise stated. Photoanodes were aged before use by placing in a solution of 0.1 M $LiClO_4$ in acetonitrile overnight. Aging the electrodes allows for stable measurements free from time-dependent effects observed in the first 12−18 h after the electrode is placed in contact with the electrolyte.[26] Open-circuit voltage decay measurements were performed by monitoring the voltage versus time response when the cell is switched to open-circuit conditions from a potentiostatically controlled applied potential on the TiO_2 electrode. All electrochemical measurements were performed in the dark with an Autolab PGSTAT 126N.

RESULTS AND DISCUSSION

1. Measurements. Current density versus applied potential, $J-E$, measurements were performed for DSSCs employing $[Co(Me_2bpy)_3]^{3+/2+}$ and $[Ru(bpy)_2(MeIm)_2]^{3+/2+}$ redox shuttles in the dark. Figure 1a shows representative $J-E$ plots using a single TiO_2 nanoparticle electrode in contact with both electrolytes.

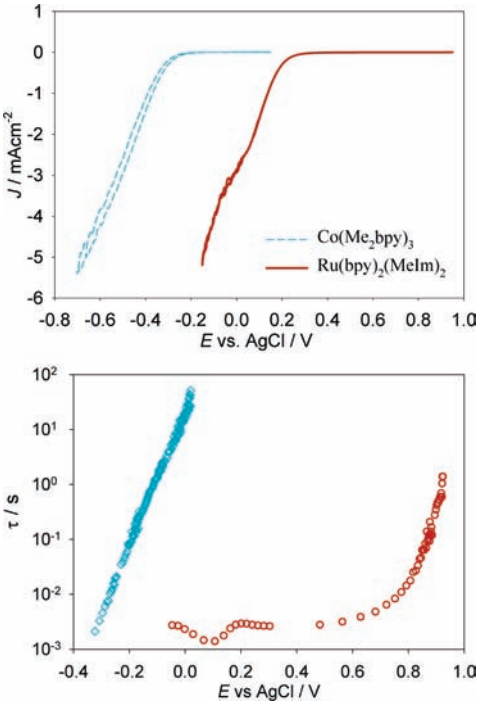

Figure 1. (a) Current density versus applied potential curves and (b) lifetimes versus potential plots for DSSCs utilizing $[Co(Me_2bpy)_3]^{3+/2+}$ (blue, − − −/◇) and $[Ru(bpy)_2(MeIm)_2]^{3+/2+}$ (red, −/○) redox shuttles.

dx.doi.org/10.1021/ja201333u |*J. Am. Chem. Soc.* 2011, 133, 8264–8271

For reference, the formal potentials of $[Co(Me_2bpy)_3]^{3+/2+}$ and $[Ru(bpy)_2(MeIm)_2]^{3+/2+}$ were measured to be 0.08 and 0.89 V vs AgCl, respectively. The dark $J-E$ curve for $[Co(Me_2bpy)_3]^{3+/2+}$ is characteristic for a DSSC utilizing cobalt-based redox shuttles.[21,26,27,31−34] The dark current density at more negative potentials deviated from the expected exponential dependence due to the increasing diffusion resistance of the electrolyte.[11] Substantially larger dark current density was found at a given potential when $[Ru(bpy)_2(MeIm)_2]^{3+/2+}$ was employed as the redox shuttle. Because the dark current density is a measure of recombination, this indicates that recombination is much faster to $[Ru(bpy)_2(MeIm)_2]^{3+/2+}$ as compared to $[Co(Me_2bpy)_3]^{3+/2+}$.[13,15,35]

Another way to compare rates of recombination is through determinations of the lifetimes, τ_n.[9,11,26,27] Lifetimes of DSSCs employing $[Co(Me_2bpy)_3]^{3+/2+}$ and $[Ru(bpy)_2(MeIm)_2]^{3+/2+}$ were measured using the open-circuit voltage decay technique.[19,36] Because this measurement is made at open circuit, and represents the average time a free electron survives before recombining, the results do not depend on any variation of the quasi-Fermi level, $\mathbf{E}_F$, in the film, whereas the Fermi level may not be completely constant in the dark current density measurements.[37] The open circuit voltage, V_{oc}, decay can be transformed into the lifetime by:[19]

$$\tau_n = -\frac{k_B T}{q}\left(\frac{dV_{oc}}{dt}\right)^{-1} \quad (1)$$

were k_B is the Boltzmann constant, T is temperature, q is the elementary charge, and t is time. Lifetimes versus open circuit potential plots for DSSCs employing $[Co(Me_2bpy)_3]^{3+/2+}$ and $[Ru(bpy)_2(MeIm)_2]^{3+/2+}$ are displayed in Figure 1b. The lifetime for the cell with $[Co(Me_2bpy)_3]^{3+/2+}$ shows the typical semilogarithmic dependence on potential. Strikingly, however, the lifetime for $[Ru(bpy)_2(MeIm)_2]^{3+/2+}$ couple is highly nonlinear and appears parabolic. The concentration of $[Ru(bpy)_2(MeIm)_2]^{3+}$ was varied by a factor of 3, and the lifetime shifted proportionally. Larger concentrations were not possible due to the limited solubility, and lower concentrations resulted in concentration polarization effects. Nevertheless, the concentration dependence of the lifetime demonstrates that recombination is first order in acceptor species.

Bisquert has suggested that recombination from surface states should lead to such a parabolic shape of the lifetime.[22] To the best of our knowledge, however, such a parabolic lifetime has not been observed experimentally when care is taken to passivate the back FTO electrode.[28] The vast majority of research reports on DSSCs have relied on the I_3^-/I^- redox shuttle, which may preclude observation of such parabolic lifetimes due to the particularly complicated electrochemistry of this couple.[11,16] Use of outersphere redox shuttles, however, allows for substantial variations in recombination rates and should additionally be more straightforward to interpret.[11] Below we develop a model to quantitatively describe recombination to these outer-sphere redox shuttles.

2. Modeling. The lifetime of electrons in the TiO_2 can be expressed as a function of the concentration of electrons, n, at a given quasi-Fermi level, $\mathbf{E}_F$, to the rate at which they are being lost, which in the dark is simply the recombination rate, U, at $\mathbf{E}_F$. Defining values for both $n(\mathbf{E}_F)$ and $U(\mathbf{E}_F)$ therefore allows for the use of the following equation to calculate the lifetime:[9]

$$\tau_n(\mathbf{E}_F) = \frac{\partial n(\mathbf{E}_F)/\partial \mathbf{E}}{\partial U(\mathbf{E}_F)/\partial \mathbf{E}} \quad (2)$$

a. Electron Concentration. The concentration of electrons may be broken down into free electrons (those which are in the conduction band), $n_{cb}(\mathbf{E}_F)$, and those residing in localized trap states, $n_t(\mathbf{E}_F)$. The concentration of conduction band electrons is dependent on the quasi-Fermi level according to:

$$n_{cb}(\mathbf{E}_F) = N_c \exp\left[\frac{\mathbf{E}_{cb} - \mathbf{E}_F}{k_B T}\right] \quad (3)$$

where N_c is the effective density of states in the conduction band, and $\mathbf{E}_{cb}$ is the energy of the conduction band minimum. A value of $\mathbf{E}_{cb}/q \approx -0.7$ V vs Ag/AgCl was used from literature data of anatase TiO_2 nanoparticle electrodes in contact with 0.1 M Li^+ in acetonitrile.[38] The effective density of states in the conduction band was determined using the effective electron mass of $m_e^* = 10m_e$, providing a value of $N_c = 8 \times 10^{20}$ cm^{-3}.[39,40]

For trap states, the concentration of electrons in the TiO_2 given a certain Fermi-level is determined by integrating the density of trap states, $g(\mathbf{E})$, multiplied by the occupancy of those traps. The trap state occupancy is described by the Fermi−Dirac function, $f(\mathbf{E} - \mathbf{E}_F)$:

$$f(\mathbf{E} - \mathbf{E}_F) = \frac{1}{1 + \exp(\mathbf{E} - \mathbf{E}_F/k_B T)} \quad (4)$$

Only electrons in traps with an energy between the solution (zero) potential, $E_{f,0}$, and the conduction band are expected to contribute to recombination. The total concentration of electrons in trap states in the energy range $qE_{f,0} < \mathbf{E} < \mathbf{E}_{cb}$ is therefore given by

$$n_t(\mathbf{E}_F) = \int_{qE_{f,0}}^{\mathbf{E}_{cb}} g(\mathbf{E}) f(\mathbf{E} - \mathbf{E}_F)\, d\mathbf{E} \quad (5)$$

The distribution of trap states can be determined experimentally through capacitance measurements. Figure 2a shows a typical cyclic voltammogram of a TiO_2 nanoparticle electrode in an electrochemically inert electrolyte. The small current peak at a potential of −0.3 V, present only in the first scan, has been identified in the literature as monoenergetic surface states.[41,42] Boschloo et al. have measured these states spectroelectrochemically to rule out the possibility that this peak is a result of contamination reduction.[41] The larger current at more negative potentials is due to the charging of an exponential distribution of trap states tailing off below the conduction band edge.[42−45] The current density can be transformed to a capacitance, C_μ, by

$$J = L(1-p)sC_\mu \quad (6)$$

where L is the film thickness, p is the porosity, and s is the scan rate.[42] Figure 3b shows a plot of $\ln(C_\mu)$ versus E. The capacitance peak associated with the monoenergetic surface states, near $E = -0.3$ V, as well as the exponential distribution of trap states are more apparent in this plot. The total density of trap states can thus be separated into two components: exponentially distributed trap states, $g_{exp}(\mathbf{E})$, and monoenergetic surface states, $g_{s,me}(\mathbf{E})$.

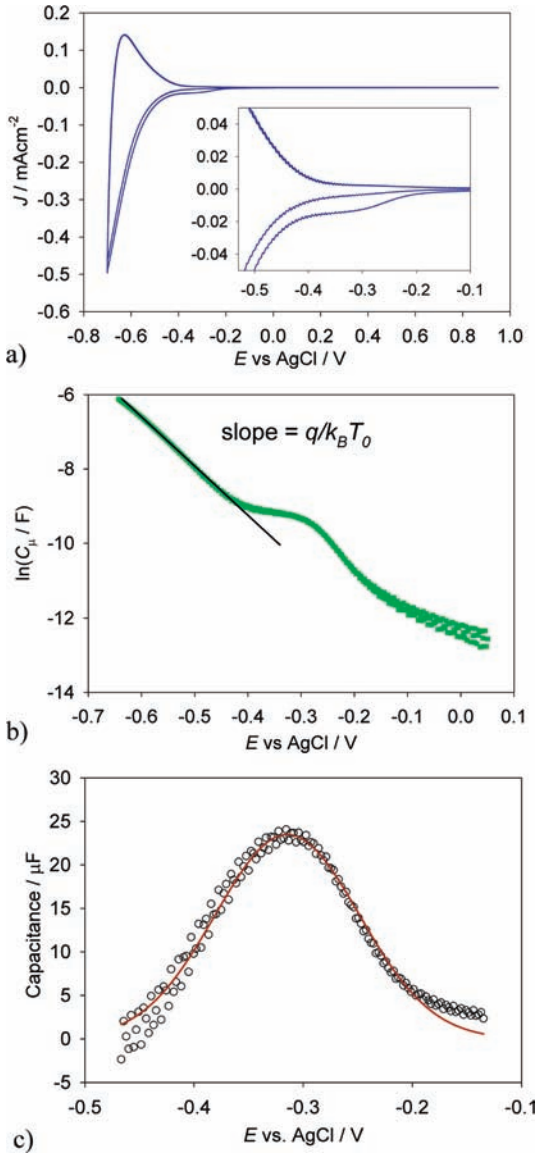

Figure 2. (a) Cyclic voltammogram and (b) plot of $\ln(C_\mu)$ versus potential for a TiO_2 electrode in a blocking electrolyte composed of 0.1 M $LiClO_4$ in acetonitrile. (c) The difference between the measured total capacitance and the fitted exponential capacitance (○). Also shown is the result of fitting the capacitance difference to a Gaussian (red line).

The exponentially distributed density of trap states in TiO_2 has been well established to be described by[7,44,46,47]

$$g_{exp}(\mathbf{E}) = \frac{N_{exp}}{k_b T_0} \exp\left[\frac{qE - \mathbf{E}_{cb}}{k_b T_0}\right] \quad (7)$$

where N_{exp} is the total density of the exponential distribution of trap states, and T_0 is a characteristic parameter with temperature units describing the depth of the trap state distribution. The tailing parameter is sometimes described in literature as m_c, a parameter with energy units that can be interchanged by $m_c = k_B T_0$ or by a unitless coefficient $\alpha = T/T_0$.[44,46] The slope of the $\ln(C_\mu)$ data can be used to determine the T_0 parameter from slope = $q/k_b T_0$.[42] A fit of the capacitance data to eq 7, shown in Figure 2b, produced a value of 850 K for T_0. This value is in good agreement with literature values, which range

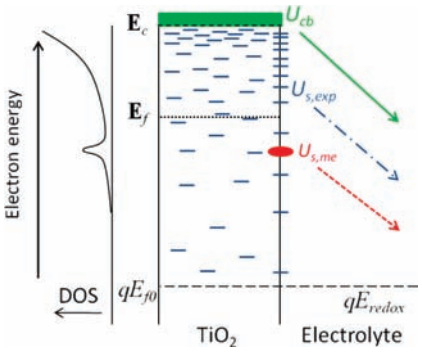

Figure 3. Energy diagram displaying the distribution of localized states and recombination from the conduction band (green —), from an exponential distribution of surface states (blue — · — · —), and from a monoenergetic distribution of states (red - - -). $qE_{f,0}$ is the quasi-Fermi level in the dark equilibrated with the redox potential of the redox shuttle, E_{redox}, $\mathbf{E}_{cb}$ is the conduction band energy, and $\mathbf{E}_F$ is the Fermi energy.

from 550 to 950 K.[7,46,48,49] An estimate of N_{exp} was obtained from the fitted capacitance data as shown in Figure 2b. The data were integrated from $\mathbf{E}_{cb}$ to $E_{f,0}$, which produced a value of $N_{exp} \approx 1.7 \times 10^{19}$ cm^{-3}, in good agreement with literature values.[7,41,44]

The monoenergetic surface states were modeled using a normalized Gaussian function:

$$g_{s,me}(\mathbf{E}) = \frac{N_{s,me}}{\sqrt{2\pi\sigma^2}} \exp\left[\frac{-(\mathbf{E} - qE_{s,me})^2}{2\sigma^2}\right] \quad (8)$$

where $N_{s,me}$ is the total density of monoenergetic surface states, $E_{s,me}$ is the potential at the center of the Gaussian function, and σ describes the width of the distribution. Approximate values for both $N_{s,me}$ and σ were obtained by integrating the difference of the capacitance measured by cyclic voltammetry and the fitted exponential capacitance, $C_{exp,fit}$, shown in Figure 2c, and determined to be 4.86×10^{17} cm^{-3} and 66 meV, respectively. We note, however, that the values derived from these measurements and fits were found to be somewhat variable between films. Further, the center of this distribution, $E_{s,me}$, shifts more positive with slower scan rates as expected. Thus, a more positive value than is indicated in Figure 2c was used for modeling purposes as shown in Table 1.

b. Recombination Rate. Recombination is comprised of electron transfer from TiO_2 to the oxidized form of the redox shuttle. In general, the equation for recombination density due to electron transfer is

$$U(\mathbf{E}_F) = [A]n(\mathbf{E}_F)k_{et}(\mathbf{E}) \quad (9)$$

where [A] is the concentration of acceptor species dissolved in solution, $n(\mathbf{E}_F)$ is the concentration of electrons able to participate in recombination, and $k_{et}(\mathbf{E})$ is the electron-transfer rate constant. In principle, any electron that is near the surface in a state higher in energy than qE_{redox} should be able to participate in recombination. The total rate of recombination is then the sum of all recombination reactions. Because we have identified three types of states containing electrons in the section above, we consider three sources of recombination here: electron transfer from (1) the conduction band, U_{cb}, (2) the exponential distribution of surface states, $U_{s,exp}$, and (3) the monoenergetic band of

dx.doi.org/10.1021/ja201333u |J. Am. Chem. Soc. 2011, 133, 8264–8271

surface states, $U_{s,me}$, displayed in Figure 3. Use of eq 9 allows us to write separate equations for each source of recombination using the proper expressions for $n(\mathbf{E}_F)$ and $k_{et}(\mathbf{E})$.

Recombination resulting from direct electron transfer from the conduction band follows the equation:

$$U_{cb}(\mathbf{E}_F) = [A]V_f n_{cb}(\mathbf{E}_F)k_{et,cb} \quad (10)$$

where $k_{et,cb}$ is the electron transfer rate constant and V_f is the volume fraction of electrons in the conduction band near enough to the surface to participate in electron transfer. An expression for $n_{cb}(\mathbf{E}_F)$ was presented above (eq 3). The volume fraction is determined by the effective coupling length of the acceptor species in the semiconductor electrode. Lewis and co-workers used a coupling length of 0.3 nm to estimate rate constants for electron transfer at semiconductor electrodes, which corresponds to the approximate width of one gold atom.[50] If the electronic coupling is strong, it has been estimated that adiabatic charge transfer can occur for species up to a nanometer from the electrode surface, which would correspond to a coupling length of 1 nm.[50,51] Because there is no clear experimental evidence to support an exact value for V_f at this time, we assume that electrons within 1 nm of the surface of the nanoparticle can participate in recombination, and thus $V_f = 0.27$ for the 20 nm in diameter nanoparticles used. We note that if a smaller coupling length were used in the calculation, it would produce a smaller V_f, which would result in an increase in the electron lifetime. For example, using a coupling length of 0.3 nm, instead of 1 nm, would produce $V_f = 0.09$ and increase the calculated lifetime by a factor of 3 (see the Supporting Information).

Because electrons are all coming from the same energy, the conduction band minimum, the rate constant has a single value, and the potential dependence of recombination is contained in $n_{cb}(\mathbf{E}_F)$. The rate constant has been established to follow the relationship described using Marcus theory:[52,53]

$$k_{et,cb} = k_{et,max} \exp\left[\frac{-(\Delta G + \lambda)^2}{4\lambda k_B T}\right] \quad (11)$$

where $\Delta G = \mathbf{E}_{cb} - qE_{redox}$ is the driving force of electron transfer, and λ is the reorganization energy. The prefactor $k_{et,max}$ is the rate constant at optimum exoergicity, obtained when $-\Delta G^{\circ\prime} = \lambda$. Values of $k_{et,max}$ have been estimated theoretically, and confirmed experimentally, to be approximately 10^{-17}–10^{-16} cm^4 s^{-1}.[52−54] In addition, the value of $k_{et,max}$ is expected to be a weak function of the reorganization energy ($k_{et,max} \propto \lambda^{-1/2}$). Making this correction, we used a value of $k_{et,max} = 6 \times 10^{-17}$ cm^4 s^{-1} for $[Co(Me_2bpy)_3]^{3+/2+}$ and 1.2×10^{-16} cm^4 s^{-1} for $[Ru(bpy)_2(MeIm)_2]^{3+/2+}$. Determination of the reorganization energies is described below.

Recombination resulting from electron transfer from surface states requires a more elaborate definition. To quantify the rate of recombination, the contributions from all occupied surface states must be included. The total density of electron transfer at a given quasi-Fermi level, again only considering surface states in the energy range $qE_{f0} < \mathbf{E} < \mathbf{E}_{cb}$, is described by

$$U_s(\mathbf{E}_F) = [A]\int_{qE_{f,0}}^{\mathbf{E}_{cb}} f(\mathbf{E} - \mathbf{E}_F)\left[(g_{s,exp}(\mathbf{E}) + g_{s,me}(\mathbf{E})\right]k_{et,s}(\mathbf{E})\, d\mathbf{E} \quad (12)$$

where $g_{s,exp}(\mathbf{E})$ is the density of exponentially distributed states at the electrode surface, and $k_{et,s}(\mathbf{E})$ is the electron-transfer rate constant from a surface state at energy $\mathbf{E}$. We assume that the rate constant is strictly a function of energy and thus independent of the type of surface state. We note, however, that it is possible that the electronic coupling can differ between types of surface states and acceptor species, which would affect the values of $k_{et,s}(\mathbf{E})$ for these states. The electron-transfer rate constants for transfer from surface states are dependent on the difference between the energy of the surface state, $\mathbf{E}$, and the solution qE_{redox}, according to:[55,56]

$$k_{et,s}(\mathbf{E}) = k_{et,max} \exp\left[\frac{-(\mathbf{E} - qE_{redox} + \lambda)^2}{4\lambda k_B T}\right] \quad (13)$$

The density of states of the monoenergetic surface states was presented above. Assuming that the surface (or near surface) states have the same distribution as the bulk trap states, the exponentially distributed density of trap states at (or near) the TiO_2 surface, $g_{s,exp}(\mathbf{E})$, can be described by the volume fraction, V_f, of bulk traps near enough to the surface of the nanoparticle to participate in electron transfer time:

$$g_{s,exp}(\mathbf{E}) = V_f g_{exp}(\mathbf{E}) \quad (14)$$

There is no definitive evidence that the distribution of trap states is evenly distributed spatially throughout the nanoparticle. In fact, it has been suggested that trap states are located preferentially at the nanoparticle surface.[57] A distribution of trap states having a higher concentration nearer to the surface would produce a larger $g_{s,exp}(\mathbf{E})$ and concomitant shorter lifetimes. We note that if a lower value for V_f were employed as described above, the decreased lifetimes could be offset by the surface-concentrated trap states. Any error on the value of either of these parameters would result in a proportional minor shift in the magnitude of the calculated lifetimes (up to a factor of 3); however, the shape of the lifetimes will be unaffected. Plots of lifetimes demonstrating this can be seen in the Supporting Information. For simplicity, we assume a homogeneous spatial distribution of trap states and an effective coupling length of 1 nm.

c. Reorganization Energy. The total reorganization energy is a summation of the inner-sphere and outer-sphere components: $\lambda = \lambda_{in} + \lambda_{out}$. It has been shown for group VIII bipyridyl complexes $\lambda_{in} \approx 0$ for the M^{2+} to M^{3+} transition or vice versa, allowing for the use of the approximation $\lambda = \lambda_{out}$.[58] A theoretical value for λ_{out} for a redox couple at a TiO_2 interface can be calculated by:[59−63]

$$\lambda_{out} = \frac{(\Delta z q)^2}{8\pi\varepsilon_0}\left[\frac{1}{a}\left(\frac{1}{n_{sol}^2} - \frac{1}{\varepsilon_{sol}}\right) - \frac{1}{2R_e}\left(\frac{1}{n_{sol}^2}\left(\frac{n_{TiO_2}^2 - n_{sol}^2}{n_{TiO_2}^2 + n_{sol}^2}\right) - \frac{1}{\varepsilon_{sol}}\left(\frac{\varepsilon_{TiO_2} - \varepsilon_{sol}}{\varepsilon_{TiO_2} + \varepsilon_{sol}}\right)\right)\right] \quad (15)$$

where Δz is the change in charge of the acceptor species, a is the radius of the reactant, n_{sol} and n_{TiO2} are the refractive index of acetonitrile (1.3442)[64] and anatase TiO_2 (2.54),[64] respectively, ε_{sol} and ε_{TiO2} are the static dielectric constants of the acetonitrile (36)[65] and anatase TiO_2 (114),[40,66] respectively, and R_e is the distance from the acceptor to the electrode. Using $a = R_e = 0.65$ nm results in a value of $\lambda_{out} = 0.41$ eV, which was used as λ for $[Ru(bpy)_2(MeIm)_2]^{3+/2+}$.[67]

Cobalt bipyridyl redox couples, however, are known to have significant innersphere reorganization energies. The inner-sphere

reorganization energy at a semiconductor electrode is one-half of the value derived from a self-exchange reaction, $\lambda_{se,in}$, because one-half as many molecules participate in each electron transfer. The total reorganization energy is therefore given by $\lambda = \lambda_{se,in}/2 + \lambda_{out}$. The $\lambda_{se,in}$ has been determined previously to be 2.04 eV.[52] Using eq 15, with $a = R_e = 0.68$ nm, produces a value of $\lambda_{out} = 0.39$ eV.[67] The total reorganization energy for $[Co(Me_2bpy)_3]^{3+/2+}$ is therefore (2.04 eV)/2 + 0.39 eV = 1.41 eV.

d. Calculated Lifetimes. Introducing the expressions developed above for electron concentration and recombination rates into eq 2 produces the following general expression for electron lifetime:

$$\tau_n(\mathbf{E}_F) = \frac{\partial\left(N_c \exp\left[\frac{\mathbf{E}_{cb}-\mathbf{E}_F}{k_B T}\right] + \int_{\mathbf{E}_{f,0}}^{\mathbf{E}_{cb}} f(\mathbf{E}-\mathbf{E}_F)[(g_{exp}(\mathbf{E}) + g_{s,me}(\mathbf{E})]\,d\mathbf{E}\right)/\partial\mathbf{E}}{\partial\left([A]\left(V_f N_c \exp\left[\frac{\mathbf{E}_{cb}-\mathbf{E}_F}{k_B T}\right] k_{et,cb} + \int_{\mathbf{E}_{f,0}}^{\mathbf{E}_{cb}} f(\mathbf{E}-\mathbf{E}_F)[(g_{s,exp}(\mathbf{E}) + g_{s,me}(\mathbf{E})]k_{et,s}(\mathbf{E})\,d\mathbf{E}\right)\right)/\partial\mathbf{E}} \quad (16)$$

Table 1. Parameters Used for Full Model of Lifetimes Given in Eq 16

parameter	value used for Co	value used for Ru
$E_{f,0}$/V vs AgCl/Ag	0.080	0.890
$E_{ss,me}$/V vs AgCl/Ag	−0.16	−0.16
$\mathbf{E}_{cb}/q$/V vs AgCl/Ag	−0.7	−0.7
N_c/cm^{-3}	8×10^{20}	8×10^{20}
N_b/cm^{-3}	1.73×10^{19}	1.73×10^{19}
$N_{s,me}$/cm^{-3}	1×10^{16}	1×10^{16}
T/K	295	295
T_0/K	850	850
$k_{et,max}$/cm^4 s^{-1}	1.2×10^{-16}	6×10^{-17}
σ/eV	0.08	0.08
λ/eV	1.41	0.41
[A]/cm^{-3}	1.20×10^{19}	1.20×10^{19}

Equation 16 was used to calculate the electron lifetimes using the parameters displayed in Table 1. Figure 4a shows the experimental lifetimes of $[Ru(bpy)_2(MeIm)_2]^{3+/2+}$ with the results from the calculated lifetimes superimposed. The calculated lifetimes (red −) are in excellent agreement with the experimental data.

Modifications of the model further allows for the identification of the source of recombination that dominates the measured lifetimes. For example, removing the contribution of electron transfer from conduction band electrons to recombination has no effect on the calculated lifetimes. This indicates that conduction band recombination is negligible and surface state recombination is dominant when using $[Ru(bpy)_2(MeIm)_2]^{3+/2+}$. This result is consistent with recombination from the conduction band being in the Marcus inverted region as expected for this couple. Alternatively, removing the contribution of the

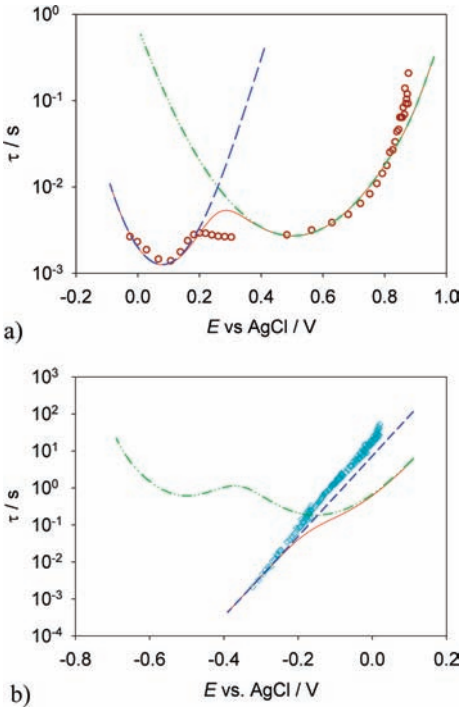

Figure 4. Experimental and modeled lifetimes for both (a) $[Ru(bpy)_2(MeIm)_2]^{3+/2+}$, experimental (○), full model (red line), model without $U_{s,me}$ (green − · · −), and model without $U_{s,exp}$ (blue − − −), and (b) $[Co(Me_2bpy)_3]^{3+/2+}$, experimental (◇), full model (red line, −), without surface state recombination (blue line, − − −), and without conduction band recombination (green line, − · · −).

monoenergetic surface states to recombination produces a parabolic lifetime with a single minimum located near 0.49 V. We can therefore attribute the experimental minimum in the lifetime at 0.49 V to recombination from the exponential distribution of surface states. This minimum occurs near where $-\Delta G = \lambda$, and thus the $k_{et}(\mathbf{E})$ function reaches its maximum. The minimum in lifetime is shifted slightly from λ, however, due to the contribution of the increasing $g_s(\mathbf{E})$ function to the overall rate of recombination. Finally, removing the contribution of the exponential distribution of surface states to recombination produces a parabolic lifetime with a single minimum located near 0.05 V. We can therefore attribute the experimental minimum in the lifetime at 0.05 V to recombination from the monoenergetic surface states. The minimum in lifetime is near the energetically center of the monoenergetic surface states, but is shifted positive due to the sharply decreasing $k_{et}(\mathbf{E})$ function with more negative potentials.

The full model using $[Co(Me_2bpy)_3]^{3+/2+}$ results in a reasonable fit over part of the experimental data, but deviates at more positive potentials, shown in Figure 4b. When the contribution to recombination from the monoenergetic surface states is removed from the model, the calculated lifetimes are in excellent agreement with the experimental results. Further removal of recombination from the exponential distribution of surface states does not significantly change the modeled lifetime, and thus only one line was included in Figure 4b for clarity. It is interesting that the monoenergetic surface states appear to contribute to recombination to $[Ru(bpy)_2(MeIm)_2]^{3+}$, but not to $[Co(Me_2bpy)_3]^{3+}$. In our previous work, we have reported linear (semilogarithmic) lifetimes for an array of cobalt polypyridyl redox shuttles, similar to the data presented here.[26,27] Peter and co-workers also reported

dx.doi.org/10.1021/ja201333u |J. Am. Chem. Soc. 2011, 133, 8264–8271

linear (semilogarithmic) lifetimes to the $[Co(dbbip)_2]^{3+/2+}$ (dbbip = 2,6-bis(1′-butylbenzimidazol-2′-yl)pyridine) redox shuttle, in agreement with our measurements. The difference may be explained by the cobalt-based redox shuttles coupling weaker to the monoenergetic surface states as compared to the ruthenium-based redox shuttle. Hupp and co-workers, however, reported nonlinear (semilogarithmic) lifetimes for a series of cobalt-based redox shuttles, which appears to be consistent with our model including the monoenergetic surface states.[21] As noted above and reported by others, we have found a fairly large variance in the magnitude of the monoenergetic states' capacitance, for different electrodes and preparation procedures. Thus, differences in the nanoparticle preparation can possibly account for differences in linearity of measured lifetimes.

As mentioned, removal of recombination from surface states to $[Co(Me_2bpy)_3]^{3+/2+}$ gives excellent agreement with experimental lifetimes. Likewise, considering only recombination from surface states and removing conduction band recombination results in a failure to fit the experimental data, Figure 4b (green — · · — line). This case results once again with two parabolic components to the calculated lifetimes as with the ruthenium redox shuttle. However, due to the large increase in λ, the contributions are reversed; the minimum centered near −0.2 V results from $U_{ss,me}$, while the minimum at more negative potentials results from $U_{ss,exp}$.

CONCLUSIONS

Measurements of recombination to outer-sphere redox shuttles with widely varying E_{redox} and λ produced concomitant widely varying magnitude and shape of the electron lifetimes. To interpret this behavior, we developed a model using Marcus theory to describe recombination from three distinct sources of electrons: the conduction band, an exponential distribution of surface states, and monoenergetic surface states. The semilogarithmic plots of the lifetimes were linear when $[Co(Me_2bpy)_3]^{3+/2+}$ was the redox shuttle. This behavior is in accord with our model when recombination is strictly from the conduction band. These results are in good agreement with our previous observations and essentially all literature reports using I_3^-/I^-. It is worth noting that surface state recombination is still expected to occur; however, because the rate is lower as compared to recombination from the conduction band, it is not observed experimentally. The semilogarithmic plots of the lifetimes were parabolic when $[Ru(bpy)_2(MeIm)_2]^{3+/2+}$ was the redox shuttle. This behavior is in accord with our model when recombination is strictly from the surface states. Recombination from the conduction band is also still expected to occur; however, in this case, we believe it to be in the Marcus inverted region and thus significantly slower as compared to recombination from surface states. The parabolic lifetimes are also in good agreement with Bisquert's predictions of surface state recombination.[22] To the best of our knowledge, however, this is the first definitive experimental verification of surface state dominated recombination in DSSCs.

It is well-known that one strategy to achieve significantly higher efficiency DSSCs is to use redox shuttles with more positive potentials to produce higher photovoltages.[12] We and others have previously demonstrated that when "slow" redox shuttles are employed, such as $[Co(X_2bpy)_3]^{3+/2+}$ or pseudohalogens, a more positive potential increases the rate of recombination, thus offsetting (at least) any gains in voltage.[14,26,27] This behavior is consistent with Marcus normal region behavior of recombination. In this work, we demonstrated that you can exploit Marcus inverted behavior by using very positive redox shuttles with slow recombination from the conduction band. Recombination from surface states, however, becomes energetically favored, and as a result even shorter lifetimes are observed. These combined results highlight the challenge faced when designing alternative redox shuttles, which are capable of exceeding the performance of the long-standing champion I_3^-/I^-. Recent exciting reports of efficient DSSCs using a variety of both outersphere and innersphere redox shuttles, however, make us optimistic that a breakthrough is on the near horizon.[24,25,68,69] Our hope is that a combination of careful systematic studies and modeling of the key processes controlling the performance of DSSCs, such as the presented herein, will help achieve this breakthrough.

ASSOCIATED CONTENT

Supporting Information. Additional figure. This material is available free of charge via the Internet at http://pubs.acs.org.

AUTHOR INFORMATION

Corresponding Author
hamann@chemistry.msu.edu

ACKNOWLEDGMENT

T.W.H. would like to thank Michigan State University for support of this work.

REFERENCES

(1) O'Regan, B.; Gratzel, M. *Nature* **1991**, *353*, 737.
(2) Nazeeruddin, M. K.; Kay, A.; Rodicio, I.; Humphry-Baker, R.; Muller, E.; Liska, P.; Vlachopoulos, N.; Gratzel, M. *J. Am. Chem. Soc.* **1993**, *115*, 6382.
(3) Gratzel, M. *J. Photochem. Photobiol., A* **2004**, *164*, 3.
(4) Chiba, Y.; Islam, A.; Watanabe, Y.; Komiya, R.; Koide, N.; Han, L. Y. *Jpn. J. Appl. Phys., Part 2* **2006**, *45*, L638.
(5) Hagfeldt, A.; Boschloo, G.; Sun, L. C.; Kloo, L.; Pettersson, H. *Chem. Rev.* **2010**, *110*, 6595.
(6) Ardo, S.; Meyer, G. J. *Chem. Soc. Rev.* **2009**, *38*, 115.
(7) Peter, L. M. *J. Phys. Chem. C* **2007**, *111*, 6601.
(8) O'Regan, B. C.; Durrant, J. R. *Acc. Chem. Res.* **2009**, *42*, 1799.
(9) Bisquert, J.; Fabregat-Santiago, F.; Mora-Sero, I.; Garcia-Belmonte, G.; Gimenez, S. *J. Phys. Chem. C* **2009**, *113*, 17278.
(10) Gratzel, M. *Inorg. Chem.* **2005**, *44*, 6841.
(11) Hamann, T. W.; Ondersma, J. W. *Energy Environ. Sci.* **2011**, *4*, 370.
(12) Hamann, T. W.; Jensen, R. A.; Martinson, A. B. F.; Van Ryswyk, H.; Hupp, J. T. *Energy Environ. Sci.* **2008**, *1*, 66.
(13) Gregg, B. A.; Pichot, F.; Ferrere, S.; Fields, C. L. *J. Phys. Chem. B* **2001**, *105*, 1422.
(14) Oskam, G.; Bergeron, B. V.; Meyer, G. J.; Searson, P. C. *J. Phys. Chem. B* **2001**, *105*, 6867.
(15) Hamann, T. W.; Farha, O. K.; Hupp, J. T. *J. Phys. Chem. C* **2008**, *112*, 19756.
(16) Boschloo, G.; Hagfeldt, A. *Acc. Chem. Res.* **2009**, *42*, 1819.
(17) Kruger, J.; Plass, R.; Gratzel, M.; Cameron, P. J.; Peter, L. M. *J. Phys. Chem. B* **2003**, *107*, 7536.
(18) Bisquert, J.; Vikhrenko, V. S. *J. Phys. Chem. B* **2004**, *108*, 2313.
(19) Zaban, A.; Greenshtein, M.; Bisquert, J. *ChemPhysChem* **2003**, *4*, 859.
(20) Schlichthorl, G.; Huang, S. Y.; Sprague, J.; Frank, A. J. *J. Phys. Chem. B* **1997**, *101*, 8141.

(21) De Vries, M. J.; Pellin, M. J.; Hupp, J. T. *Langmuir* **2010**, *26*, 9082.
(22) Bisquert, J.; Zaban, A.; Greenshtein, M.; Mora-Sero, I. *J. Am. Chem. Soc.* **2004**, *126*, 13550.
(23) Mora-Sero, I.; Gimenez, S.; Fabregat-Santiago, F.; Gomez, R.; Shen, Q.; Toyoda, T.; Bisquert, J. *Acc. Chem. Res.* **2009**, *42*, 1848.
(24) Daeneke, T.; Kwon, T.-H.; Holmes, A. B.; Duffy, N. W.; Bach, U.; Spiccia, L. *Nat. Chem.* **2011**, *3*, 211.
(25) Feldt, S. M.; Gibson, E. A.; Gabrielsson, E.; Sun, L.; Boschloo, G.; Hagfeldt, A. *J. Am. Chem. Soc.* **2010**, *132*, 16714.
(26) Ondersma, J. W.; Hamann, T. W. *J. Phys. Chem. C* **2010**, *114*, 638.
(27) Klahr, B. M.; Hamann, T. W. *J. Phys. Chem. C* **2009**, *113*, 14040.
(28) Cameron, P. J.; Peter, L. M. *J. Phys. Chem. B* **2005**, *109*, 7392.
(29) Ondersma, J. W.; Hamann, T. W. **2011**, impending publication.
(30) Hamann, T. W.; Gstrein, F.; Brunschwig, B. S.; Lewis, N. S. *Chem. Phys.* **2006**, *326*, 15.
(31) Sapp, S. A.; Elliott, C. M.; Contado, C.; Caramori, S.; Bignozzi, C. A. *J. Am. Chem. Soc.* **2002**, *124*, 11215.
(32) Nusbaumer, H.; Zakeeruddin, S. M.; Moser, J. E.; Gratzel, M. *Chem.-Eur. J.* **2003**, *9*, 3756.
(33) Cameron, P. J.; Peter, L. M.; Zakeeruddin, S. M.; Gratzel, M. *Coord. Chem. Rev.* **2004**, *248*, 1447.
(34) Nelson, J. J.; Amick, T. J.; Elliott, C. M. *J. Phys. Chem. C* **2008**, *112*, 18255.
(35) Gregg, B. A. *Coord. Chem. Rev.* **2004**, *248*, 1215.
(36) Walker, A. B.; Peter, L. M.; Lobato, K.; Cameron, P. J. *J. Phys. Chem. B* **2006**, *110*, 25504.
(37) To clarify notation used throughout this work, an italicized *E* denotes potential, while a bold **E** denotes energy.
(38) Redmond, G.; Fitzmaurice, D. *J. Phys. Chem.* **1993**, *97*, 1426.
(39) Nelson, J. *The Physics of Solar Cells*; Imperial College Press: London, 2003.
(40) Enright, B.; Fitzmaurice, D. *J. Phys. Chem.* **1996**, *100*, 1027.
(41) Boschloo, G.; Fitzmaurice, D. *J. Phys. Chem. B* **1999**, *103*, 2228.
(42) Bisquert, J.; Fabregat-Santiago, F.; Mora-Sero, I.; Garcia-Belmonte, G.; Barea, E. M.; Palomares, E. *Inorg. Chim. Acta* **2008**, *361*, 684.
(43) Kay, A.; Humphry-Baker, R.; Gratzel, M. *J. Phys. Chem.* **1994**, *98*, 952.
(44) Fabregat-Santiago, F.; Mora-Sero, I.; Garcia-Belmonte, G.; Bisquert, J. *J. Phys. Chem. B* **2003**, *107*, 758.
(45) Zhang, Z.; Zakeeruddin, S. M.; O'Regan, B. C.; Humphry-Baker, R.; Gratzel, M. *J. Phys. Chem. B* **2005**, *109*, 21818.
(46) van de Lagemaat, J.; Frank, A. J. *J. Phys. Chem. B* **2000**, *104*, 4292.
(47) Boschloo, G.; Hagfeldt, A. *J. Phys. Chem. B* **2005**, *109*, 12093.
(48) Konenkamp, R. *Phys. Rev. B* **2000**, *61*, 11057.
(49) Fisher, A. C.; Peter, L. M.; Ponomarev, E. A.; Walker, A. B.; Wijayantha, K. G. U. *J. Phys. Chem. B* **2000**, *104*, 949.
(50) Royea, W. J.; Fajardo, A. M.; Lewis, N. S. *J. Phys. Chem. B* **1998**, *102*, 3653.
(51) Feldberg, S. W.; Sutin, N. *Chem. Phys.* **2006**, *324*, 216.
(52) Hamann, T. W.; Gstrein, F.; Brunschwig, B. S.; Lewis, N. S. *J. Am. Chem. Soc.* **2005**, *127*, 13949.
(53) Hamann, T. W.; Gstrein, F.; Brunschwig, B. S.; Lewis, N. S. *J. Am. Chem. Soc.* **2005**, *127*, 7815.
(54) Royea, W. J.; Fajardo, A. M.; Lewis, N. S. *J. Phys. Chem. B* **1997**, *101*, 11152.
(55) Memming, R. *Semiconductor Electrochemistry*; Wiley-VCH Verlag GmbH: Weinheim, Germany, 2001.
(56) Lewis, N. S. *Z. Phys. Chem.* **1999**, *212*, 161.
(57) Kopidakis, N.; Neale, N. R.; Zhu, K.; van de Langemaat, J.; Frank, A. J. *Appl. Phys. Lett.* **2005**, *87*, 202106.
(58) Biner, M.; Burgi, H.-B.; Ludi, A.; C., R. *J. Am. Chem. Soc.* **1992**, *114*, 5197.
(59) Kuciauskas, D.; Freund, M. S.; Gray, H. B.; Winkler, J. R.; Lewis, N. S. *J. Phys. Chem. B* **2001**, *105*, 392.
(60) Marcus, R. A. *J. Chem. Phys.* **1965**, *43*, 679.
(61) Marcus, R. A. *Electrochim. Acta* **1968**, *13*, 995.
(62) Marcus, R. A. *J. Phys. Chem.* **1990**, *94*, 1050.
(63) Gao, Y. Q.; Georgievskii, Y.; Marcus, R. A. *J. Chem. Phys.* **2000**, *112*, 3358.
(64) *CRC Handbook of Chemistry and Physics*, 81st ed.; Lide, D. R., Ed.; CRC Press: Boca Raton, FL, 2001.
(65) Blomgren, G. E. *Nonaqueous Electrochemistry*; Marcel Dekker: New York, 1999.
(66) Rothenberger, G.; Fitzmaurice, D.; Gratzel, M. *J. Phys. Chem.* **1992**, *96*, 5983.
(67) Royea, W. J.; Hamann, T. W.; Brunschwig, B. S.; Lewis, N. S. *J. Phys. Chem. B* **2006**, *110*, 19433.
(68) Li, T. C.; Spokoyny, A. M.; She, C. X.; Farha, O. K.; Mirkin, C. A.; Marks, T. J.; Hupp, J. T. *J. Am. Chem. Soc.* **2010**, *132*, 4580.
(69) Wang, M. K.; Chamberland, N.; Breau, L.; Moser, J. E.; Humphry-Baker, R.; Marsan, B.; Zakeeruddin, S. M.; Gratzel, M. *Nat. Chem.* **2010**, *2*, 385.